Journal of Molecular Cell Biology (2022), 14(8), mjac056 https://doi.org/10.1093/jmcb/mjac056
Published online October 3, 2022

Article

Acetylation of Nup62 by TIP60 ensures accurate chromosome segregation in mitosis

Hameed Akbar[1,2], Jun Cao[1,2], Dongmei Wang[1,2], Xiao Yuan[1,2], Manjuan Zhang[1,2], Saravanakumar Muthusamy[3], Xiaoyu Song[1,3], Xu Liu[1,2], Felix Aikhionbare[3], Xuebiao Yao[1,2,*], Xinjiao Gao[1,2,*], and Xing Liu [1,2,3,*]

[1] MOE Key Laboratory for Cellular Dynamics and School of Life Sciences, University of Science and Technology of China, Hefei 230027, China
[2] CAS Center for Excellence in Molecular and Cell Sciences, Anhui Key Laboratory for Cellular Dynamics and Chemical Biology, Hefei 230027, China
[3] Morehouse School of Medicine, Atlanta, GA 30310, USA
* Correspondence to: Xing Liu, E-mail: xing1017@ustc.edu.cn; Xuebiao Yao, E-mail: yaoxb@ustc.edu.cn; Xinjiao Gao, E-mail: gaox@ustc.edu.cn

Edited by Jiarui Wu

Stable transmission of genetic information during cell division requires faithful mitotic spindle assembly and chromosome segregation. In eukaryotic cells, nuclear envelope breakdown (NEBD) is required for proper chromosome segregation. Although a list of mitotic kinases has been implicated in NEBD, how they coordinate their activity to dissolve the nuclear envelope and protein machinery such as nuclear pore complexes was unclear. Here, we identified a regulatory mechanism in which Nup62 is acetylated by TIP60 in human cell division. Nup62 is a novel substrate of TIP60, and the acetylation of Lys432 by TIP60 dissolves nucleoporin Nup62–Nup58–Nup54 complex during entry into mitosis. Importantly, this acetylation-elicited remodeling of nucleoporin complex promotes the distribution of Nup62 to the mitotic spindle, which is indispensable for orchestrating correct spindle orientation. Moreover, suppression of Nup62 perturbs accurate chromosome segregation during mitosis. These results establish a previously uncharacterized regulatory mechanism in which TIP60-elicited nucleoporin dynamics promotes chromosome segregation in mitosis.

Keywords: mitosis, spindle, Nup62, TIP60, acetylation

Introduction

The process of stable transmission of genetic information through generations of living organisms requires accurate bipolar spindle assembly to segregate chromosomes into daughter cells. Aberrant assembly and/or regulation of the mitotic spindle in human cells lead to aneuploidy and tumorigenesis (Dou et al., 2019; Liu et al., 2020; Krupina et al., 2021). To facilitate the transmission of parental genetic materials, eukaryotic cells undergo rapidly disintegration of nuclear pore complexes (NPCs) during nuclear envelope breakdown (NEBD), so that nuclear and cytoplasmic components mix to enable the formation of a bipolar mitotic spindle in mitosis. NPCs are formed by multiple copies of ∼30 distinct nucleoporins (Nups) that are organized into discernible NPC subcomplexes. Nups can be loosely grouped into three categories including Phe-Gly (FG)-repeat domain. Nups serve as interaction sites for nuclear transport receptors (Walther et al., 2003). NPC also constitutes the central Nup62 complex (Nup62–Nup58–Nup54) for mRNA export in interphase cells (Bailer et al., 2001).

Nup62 establishes direct interactions with nuclear transport factor 2 (NTF2) via its FG-repeat domain critical for the transport activity of NTF2 (Sheffield et al., 2006). In contrast, its C-terminal is responsible for facilitating the anchoring of Nup62 with other components of the subcomplex (Devos et al., 2006; Alber et al., 2007) and has been shown to interact with a transport receptor, importin β *in vitro* (Jovanovic-Talisman et al., 2009). This region has been identified to have centrosome and mitotic spindle localization (Hashizume et al., 2013). A subset of the Nup62 population has also been reported at the midbody and co-localizes with CapG protein at the end of abscission, supporting the notion of crosstalk between microtubule-based organelles and actin microfilament during cell division (Hubert et al., 2009).

Nup62 binds with the proteins having a tetratricopeptide repeat domain like PP5, FKBP52, and p23 and with the heat shock proteins like Hsp70 and Hsp90 in order to import glucocorticoid

Received March 27, 2022. Revised June 14, 2022. Accepted September 29, 2022.

receptor to the nucleus (Echeverría et al., 2009). In addition, Nup62 has been found indispensable for HIV-1 vRNA shuttling across the nuclear envelope (NE) and found inside a newly synthesized virion (Monette et al., 2011). A C-terminal subunit of the heterodimeric transmembrane protein, mucin 1, was reported to establish specific interaction with the central A/T-rich domain and indirectly with the coiled-coil domain of Nup62 (Leng et al., 2007). More recently, NSP9 (viral accessory protein of SARS-CoV-2) is reported to co-localize with Nup62 in cytoplasm thus attenuating Nup62 NPC localization and resulting in impaired translocation of p65, a subunit of NF-κB (Makiyama et al., 2022). Furthermore, Nup62 RNA interference studies have indicated G2/M arrest of HeLa cells, errors in centriole maturation and centrosome segregation, and faulty spindle orientation and chromosome alignment defects (Hashizume et al., 2013).

During mitotic entry, the activation of multiple mitotic kinases leads to the phosphorylation of numerous nuclear factors, including Nups, which contributes to NPC disassembly, chromatin condensation, disintegration of the nuclear lamina, and the release of the NE. Together with microtubule-dependent remodeling of the NE, phosphorylation-driven changes in protein interaction networks are the main drivers of NEBD (Linder et al., 2017; Martino et al., 2017). NPC disintegration leads to the release of FG-Nups and most scaffold Nups. During reformation of the nuclear compartments, NE reformation, and NPC reassembly are driven by dephosphorylation of Nups and other nuclear factors (Güttinger et al., 2009; Ungricht and Kutay, 2017). NPC assembly is spatially guided to the surface of chromatin by both the chromatin-associated Nup ELYS and the GTP-bound form of Ran (Clarke and Zhang, 2008; Bao et al., 2018). Our recent studies delineate a regulatory mechanism in which TIP60 provides a homeostatic control of Ran-GTP level for chromosome segregation in mitosis. However, the regulation of Nups by other post-translational modifications such as acetylation has remained uncharacterized.

In this study, we describe the essential and novel contribution of Nup62 acetylation in accurate chromosome segregation and spindle orientation in mitosis. Nup62 is a novel substrate of the acetyltransferase TIP60, and the acetylation of Lys432 of Nup62 releases its association from the central Nup62–Nup58–Nup54 complex. Importantly, the CDK1-elicited phosphorylation of TIP60 exhibits a similar temporal profile to that of Nup62 acetylation and complex disassembly during cell cycle, resulting in redistribution of Nup62 to mitotic spindle. Thus, acetylation-elicited redistribution of Nup62 provides a direct and perhaps evolutionarily conserved strategy to organize dynamic spindle for faithful mitosis.

Results

TIP60 is a novel interacting protein of Nup62

Our recent studies showed that TIP60 acetylates and regulates Aurora B, Hec1, and Ran to ensure an accurate formation of the mitotic spindle and error-free chromosome segregation during cell division (Mo et al., 2016; Bao et al., 2018; Zhao et al., 2019). Given the nuclear localization of TIP60 and mitotic regulation of nuclear structures, we sought to examine whether Nup62 exists in the TIP60 complex by carrying out an immunoprecipitation (IP) experiment. As shown in Figure 1A, anti-FLAG-TIP60 affinity beads isolated several polypeptides with an approximate mass ranging from 125 to 32 kDa. Our mass spectrometric analyses identified the presence of Aurora B, a characterized mitotic kinase interacting with TIP60 in mitosis (Mo et al., 2016). In addition, our analyses identified the 62-kDa polypeptide as Nup62. Western blotting analyses validated that Aurora B and Nup62 exist in the immunoprecipitates of TIP60 from mitotic cell lysates but to a lesser extent in interphase immunoprecipitates. In addition, endogenous Nup62 IP brought down TIP60 protein from mitotic cell lysates (Figure 1B, lane 4). Furthermore, a reciprocal co-IP assay was also conducted to confirm the existence of Nup62–TIP60 mutual interaction *in vivo* (Supplementary Figure S1A). Thus, we conclude that TIP60 can form a complex with Nup62 in mitotic cells.

To confirm that the association of Nup62 to TIP60 is a direct interaction between TIP60 and Nup62 rather than via other components such as Aurora B, glutathione S-transferase (GST)-TIP60 was used as an affinity matrix to pull down maltose-binding protein (MBP)-Nup62 from bacterial cell lysates. As shown in Supplementary Figure S1B, only MBP-Nup62, but not MBP tag, was absorbed by the affinity matrix (lanes 4 and 5), indicating a specific interaction between Nup62 and TIP60. Thus, we conclude that Nup62 is an interacting protein of TIP60.

TIP60 is an acetyltransferase that transiently localizes to the kinetochore upon NEBD (Mo et al., 2016; Zhao et al., 2019). We next sought to examine whether Nup62 distributes with TIP60 in the mitotic cells. As shown in Figure 1C (upper panel), TIP60 signal was readily evident at the kinetochore where it was superimposed to the signal of anti-centromere antibody (ACA) in a prophase cell (merge; red dots, see both insets). However, the degree of co-distribution of TIP60 with ACA was increased as the cell entered into prometaphase (lower panel), which was also evident from the line scans analyses (Figure 1D and E). This indicates that localization of TIP60 to kinetochore is dynamic, which is consistent with previous findings (Mo et al., 2016). In fact, co-localization analyses of TIP60 with ACA indicated that TIP60 became highly associated with the kinetochore during prometaphase (Figure 1F) when its catalytic activity was high. Besides kinetochore localization, a subset of the TIP60 population was evident at the centrosome region. As shown in Figure 1C, careful examination of Nup62 distribution related to TIP60 revealed their partial co-distribution in prophase and prometaphase (arrows in merged images). Furthermore, the co-localization of TIP60 and Nup62 vanished after prometaphase (Supplementary Figure S1C). Thus, we conclude that Nup62 interacts and co-distributes with TIP60 during the early phases of mitosis.

Characterization of TIP60–Nup62 interactions

To delineate the specific interface between Nup62 and TIP60 and to observe Nup62 subcellular distribution and its regulation, we constructed a series of deletion and truncation

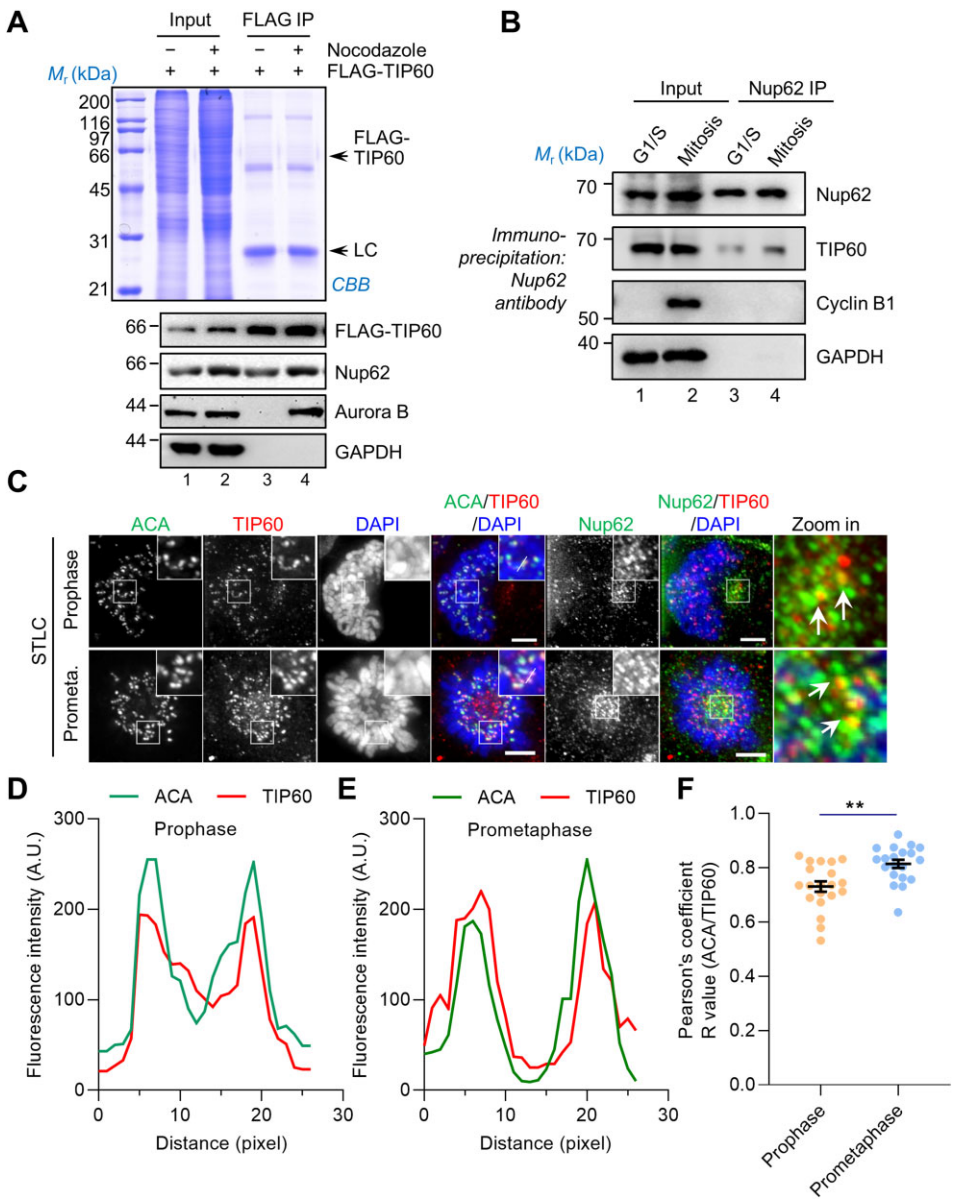

Figure 1 Nup62 is a novel interacting protein of TIP60. (**A**) Analysis of FLAG-TIP60 immunoprecipitated with M2-beads through western blotting and probing with FLAG antibody. Coomassie Brilliant Blue (CBB)-stained gel of interacting proteins immunoprecipitated with FLAG M2-resin from asynchronized or mitotic (nocodazole, 100 ng/ml, 17–18 h) FLAG-TIP60-expressing cells. The immunoprecipitates were later analyzed by mass spectrometry as well. Western blotting analyses were performed with anti-Aurora B and anti-Nup62 antibodies to annotate endogenous level of respective proteins (lower panel). (**B**) Endogenous IP assay. Endogenous Nup62 immunoprecipitates from interphase (2 mM thymidine, 17 h) or mitotic (100 ng/ml nocodazole, 16–18 h) HeLa cells were detected with antibodies against Nup62, TIP60, Cyclin B1, and GAPDH. (**C**) Immunofluorescence staining of Nup62, TIP60, and ACA in mitotic HeLa cells. DNA was stained with DAPI. Co-distribution of Nup62 with TIP60 becomes apparent at the centrosome region in prophase and prometaphase upon S-trityl-L-cysteine (STLC, a selective inhibitor of mitotic kinesin Eg5) treatment. Scale bar, 5 μm. (**D** and **E**) Line scans show the position of proteins (TIP60 and ACA) in relation to each other in prophase and prometaphase cells, respectively, and indicate fluorescence intensity along the white solid line in the ACA/TIP60 merged panel in **C**. (**F**) Pearson's correlation coefficient values for co-localization of ACA and TIP60 in prophase and prometaphase HeLa cells. The average Pearson's correlation coefficients were calculated from 10 randomly selected kinetochore in 60 prophase or prometaphase cells from three independent experiments. $^{**}P < 0.01$.

mutants of Nup62 (Figure 2A) and examined their localization in HeLa cells. As shown in Figure 2B, full-length Nup62 distributed to the NE in interphase cells and to the mitotic spindle microtubules in mitotic cells (top panel). The C-terminal region of Nup62, which contains a coiled-coil region, also distributed to the NE in interphase cells and to the mitotic spindle microtubules in mitotic cells (bottom panel). However, the N-terminal of Nup62 failed to do so (middle panel). Given the fact that deletion of C-terminal significantly perturbed Nup62 localization to the NE in interphase cells and mitotic spindle of mitotic cells, we conclude that the C-terminal of Nup62 is likely responsible for its spindle targeting, which is in accordance with the previous findings (Hashizume et al., 2013).

As Nup62 localizes to the NE during interphase and becomes associated with centrosome and mitotic spindles during mitosis, it prompted us to evaluate the temporal dynamics of Nup62 protein expression profile during cell cycle. For this purpose, we assessed the temporal profile of Nup62 levels from G1/S phase to G2/M phase and during mitosis, relative to those of Cyclin B1 and glyceraldehyde-3-phosphate dehydrogenase (GAPDH), by collecting synchronized HeLa cells for western blotting. Intriguingly, Nup62 expression profile was rather persistent during cell cycle and different from that of Cyclin B1, which became high during mitotic entry (Figure 2C, lanes 5–7). It confirmed that Nup62 expression profile is maintained throughout the cell cycle and does not change upon mitotic entry when NEBD occurs.

To determine the concrete domain(s) and physical contacts required for the Nup62–TIP60 interaction, we carried out a GST pull-down assay using GST-TIP60 as an affinity matrix to absorb the full-length MBP-Nup62 and the N-terminal or C-terminal deletion mutants from bacterial cell lysate. Immunoblotting with anti-MBP antibody confirmed a direct interaction between the Nup62 C-terminal region and TIP60 *in vitro* (Figure 2D, lane 14). This was recapitulated by our co-IP assay, in which full-length Nup62 and its C-terminal formed complex with FLAG-TIP60 exogenously expressed in HEK293T cells (Supplementary Figure S2A, lane 6). We next sought to map a specific domain of TIP60, which interacts with Nup62, using a series of TIP60 deletion mutants tagged with GFP. As illustrated in Supplementary Figure S2B, bacterially expressed MBP-Nup62 was used as affinity matrix to absorb full-length or truncated GFP-TIP60 fragments from HEK293T cell lysates. As shown in Supplementary Figure S2C, the C-terminal region of TIP60 containing MYST domain was the contact site for Nup62 (lane 14). Thus, we conclude from our biochemical characterization that TIP60 C-terminal region harboring MYST domain interacts with Nup62. In addition, Nup62 interacts with TIP60 through its C-terminal domain both *in vivo* and *in vitro*.

Nup62 is a novel substrate of TIP60

TIP60 is an important regulator for spindle plasticity and accurate chromosome segregation (Mo et al., 2016; Song et al., 2021), whereas mounting evidence demonstrated the regulation of Nup62 by mitotic phosphorylation (Martino et al., 2017). We hypothesized that TIP60 may acetylate and regulate Nup62 function. To test whether Nup62 is a substrate of TIP60, we carried out an *in vitro* acetylation assay as we previously reported (Mo et al., 2016). Specifically, FLAG-TIP60 isolated from HEK293T cells was used to acetylate recombinant MBP-Nup62 *in vitro* in the presence or absence of Ac-CoA. As shown in Figure 3A, acetylation of MBP-Nup62 was judged by western blotting analyses, which showed that Nup62 was acetylated by TIP60 (lane 3) and that the acetylation was minimized without TIP60 (lane 2). Nup62 was not acetylated by catalytically inactive TIP60 (Q377E, G380E; TIP60-DN) (lane 4), suggesting that Nup62 is a cognate substrate of TIP60 but not acetylated by other catalytic activities associated with TIP60 immunoprecipitates.

We next sought to pinpoint the acetylation sites of Nup62 that are responsible for TIP60 catalysis. Searching Phosphosite-plus database revealed that no mass spectrometry-based lysine residue was identified for acetylation. We conducted sequence alignment analyses to determine the evolutionarily conserved lysine residues in Nup62 and found that the numerous lysine residues in the coiled-coil region are conserved (Supplementary Figure S3A). In order to find out the potential lysine residues for TIP60 catalysis, we searched Nup62 in GPS-PAIL 5.0 (prediction of acetylation on internal lysine) server. Importantly, the prediction server identified Lys432 as a potential site for TIP60 catalysis (Supplementary Figure S3B). To further confirm whether this site is the substrate of TIP60 in mitosis, we performed an IP assay with mitotic HeLa cells expressing a wild-type (WT) Nup62, a non-acetylatable mutant Nup62^{K432R}, and a deletion mutant Nup62$^{\Delta CC}$. Using a pan-acetylation antibody to probe acetylated lysine, we detected strong acetylation of WT Nup62 when TIP60 enzymatic activity was not inhibited (Figure 3B, lane 1). Furthermore, we found that the acetylation level of Nup62 was abolished when Lys432 was mutated to arginine (Figure 3B, lane 2). Consistent with the substrate specificity, the acetylation was also diminished when the C-terminal coiled-coil domain (Nup62$^{\Delta CC}$) was deleted (lane 3). Importantly, treatment with the TIP60 chemical inhibitor NU9065 suppressed acetylation signals in FLAG-tagged Nup62 isolated from mitotic HeLa cells (lanes 4–6), confirming that TIP60-mediated Lys432 acetylation is a function of TIP60 in mitosis. To validate whether Nup62 acetylation exists in mitotic cells, a WT Nup62, a non-acetylatable mutant Nup62^{K432R}, and a deletion mutant Nup62$^{\Delta CC}$ were immunoprecipitated from TIP60 shRNA-transfected HeLa cells synchronized in mitosis. As shown in Figure 3C, immunoprecipitated FLAG-Nup62 acetylation was minimized in TIP60-depleted mitotic HeLa cells (lanes 1–3) but sustained in the presence of catalytically active TIP60 (lane 4).

We further evaluated whether the substrate site Lys432 at the C-terminal of Nup62 is involved in the interaction between TIP60 and Nup62. To this end, GST-TIP60 was used as an affinity matrix to absorb MBP-Nup62-CT and non-acetylatable Nup62-CT^{K432R}. As shown in Figure 3D, only WT Nup62-CT (lane 8) but not non-acetylatable Nup62-CT^{K432R} (lane 9) was absorbed by the affinity matrix, indicating the importance of Lys432 of Nup62 in association with TIP60. In addition, GST did not bind to MBP-

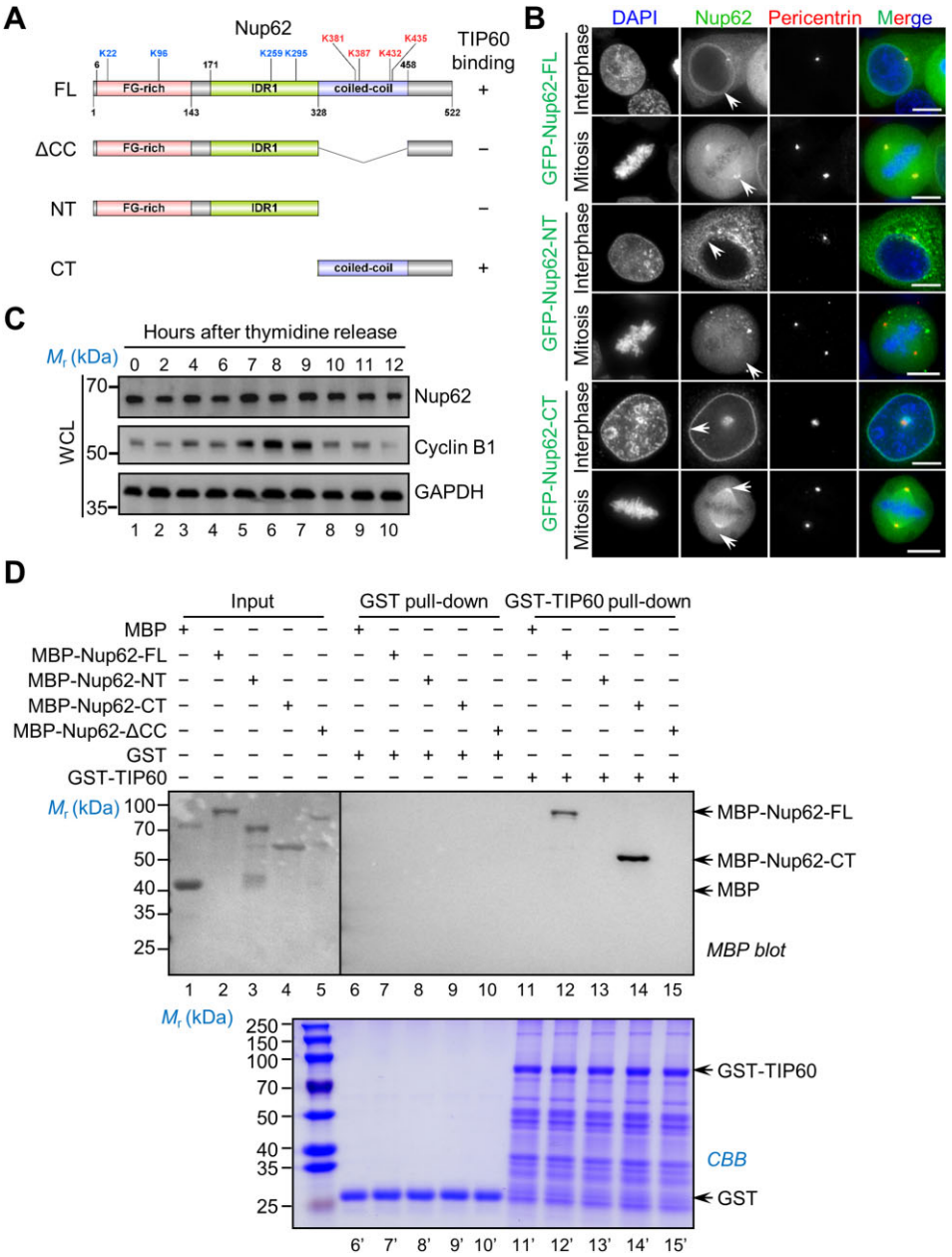

Figure 2 Nup62 interacts with TIP60 via the coiled-coil domain. (**A**) The schematic representation of different Nup62 truncations and deletion mutant generated to pin down the TIP60-binding activity. FL, full-length, aa 1–522; ΔCC, coiled-coil domain deleted mutant, Δaa 328–458; NT, N-terminal, aa 1–328; CT, C-terminal, aa 329–522. (**B**) Immunofluorescence images for localization of transiently expressed GFP-Nup62-FL, NT, and CT in interphase and mitotic Hela cells. Cells were synchronized with 2 mM thymidine for 16 h in G1/S before fixing with 4% formaldehyde or released from thymidine for 8 h to observe the protein localization in mitotic cells. Pericentrin was stained to indicate centrosome. Scale bar, 5 μm. (**C**) Temporal expression profile of Nup62 during cell cycle. Western blotting analyses of Nup62 in G1/S-synchronized HeLa cells. Note that Nup62 level is comparatively stable, unlike cyclin B1 levels that change from interphase to mitosis**.** GAPDH served as a loading control. WCL, whole-cell lysate. (**D**) *In vitro* pull-down assay between GST-TIP60 and MBP-Nup62 FL and deletion mutants. GST-TIP60-bound agarose beads were used as affinity matrices to absorb the MBP-Nup62 FL or deletion mutants purified from bacteria. The affinity matrices were subjected to western blotting analysis after extensive washes with the indicated antibodies (upper panel) or CBB staining (lower panel). The bound or absorbed fraction of MBP-Nup62-CT with GST-TIP60 is indicated with an arrow.

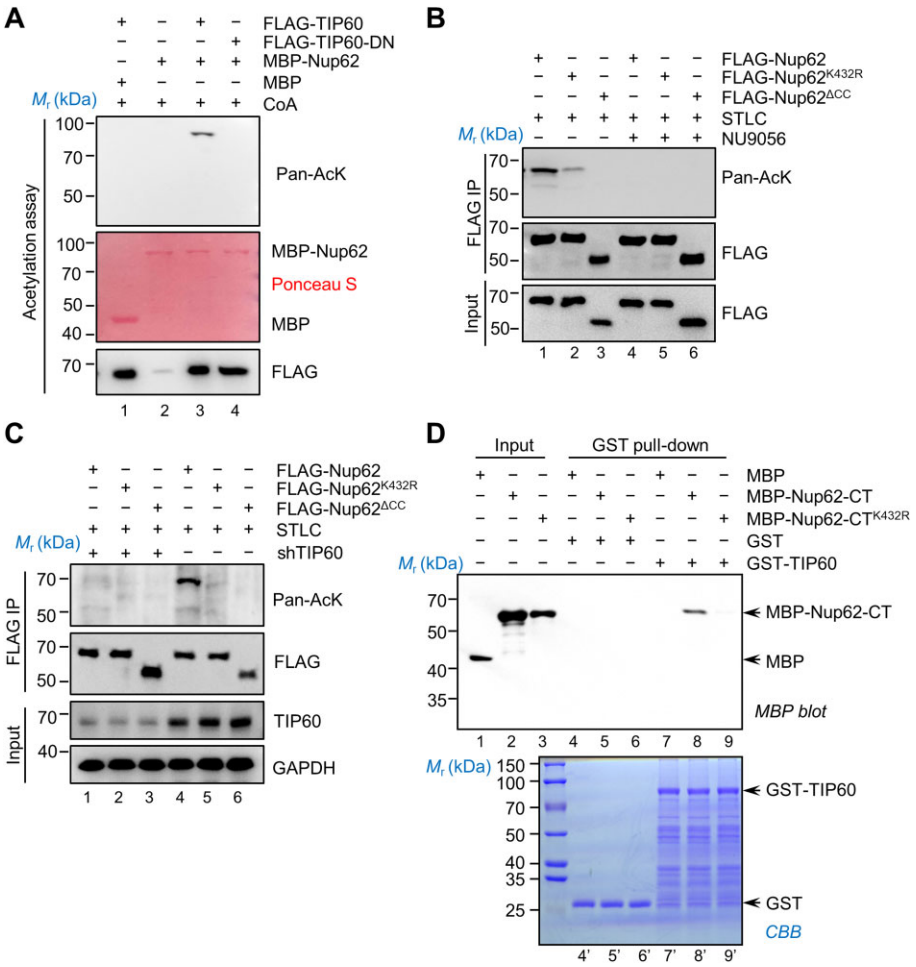

Figure 3 Lys432 located in coiled-coil domain of Nup62 is acetylated by TIP60. (**A**) *In vitro* acetylation assay between Nup62 and TIP60. FLAG-TIP60 was incubated with MBP-Nup62 in the presence of deacetylase inhibitors (TSA and NAM) and Ac-CoA for *in vitro* acetylation assay. Ac-CoA was not added in lane 1, as a negative control. The acetylation level of Nup62 was analyzed with an anti-acetyllysine antibody (acK). (**B**) HeLa cells were transfected with FLAG-tagged Nup62^{FL}, FLAG-Nup62^{K432R}, and FLAG-Nup62$^{\Delta CC}$, respectively. Cells were synchronized in G1/S with thymidine for 17 h before releasing for additional 8 h. Afterwards, cells were synchronized in mitosis by STLC for 4 h. In lanes 4–6, cells were treated with NU9056 for additional 2 h. Mitotic cells were collected by shaking off and subjected to IP with anti-FLAG M2 beads. Immunoprecipitates were analyzed with an anti-acetyllysine antibody (acK) and an anti-FLAG antibody. (**C**) G1/S-synchronized HeLa cells expressing FLAG-Nup62 (WT, K432R, or ΔCC) and depleted in TIP60 through shRNA-containing lentivirus-based system were released into mitosis for 4 h followed by treating with the Eg5 inhibitor STLC for additional 4 h. The treated cells were used to generate cell lysates for an anti-M2 IP. Immunoprecipitates were analyzed with anti-TIP60, anti-acetyllysine (acK), and anti-FLAG antibodies. (**D**) *In vitro* pull-down assay of GST-TIP60 with MBP-Nup62-CT or with non-acetylatable Nup62-CT^{K432R}. The gel was stained with CBB (lower panel). Western blotting analysis was conducted with an anti-MBP antibody (upper panel).

Nup62-CT (lane 5*)*. To evaluate the interaction of acetylation-mimicking mutant of Nup62 with TIP60, we employed another round of pull-down assay by incubation of bacterially expressed MBP-tagged Nup62^{WT} and Nup62 mutants (Nup62^{K432R} and Nup62^{K432Q}) with GST-TIP60 affinity matrix. Interestingly, acetylation-mimicking Nup62 acted similarly to Nup62^{WT} as they were retained by GST-TIP60 affinity matrix (Supplementary Figure S3C, lanes 6 and 8). In contrast, a non-acetylatable mutant Nup62^{K432R} was unable to bind to GST-TIP60 affinity matrix (lane 7). Furthermore, co-IP assay was employed to confirm the independent physical binding of Nup62-CT via Lys432 with TIP60 in a cellular system (Supplementary Figure S3D). Thus, we conclude that Nup62-CT is an interacting partner and substrate of TIP60.

Nup62 is essential for accurate chromosome segregation

Having demonstrated an enzymatic association between TIP60 and Nup62, we sought to determine the functional relevance of Nup62 during mitosis using live cell imaging of HeLa cells expressing GFP-Nup62 and GFP-Nup62$^{\Delta CC}$. To systematically assess the function of Nup62 in faithful mitotic progression, we employed a siRNA to suppress

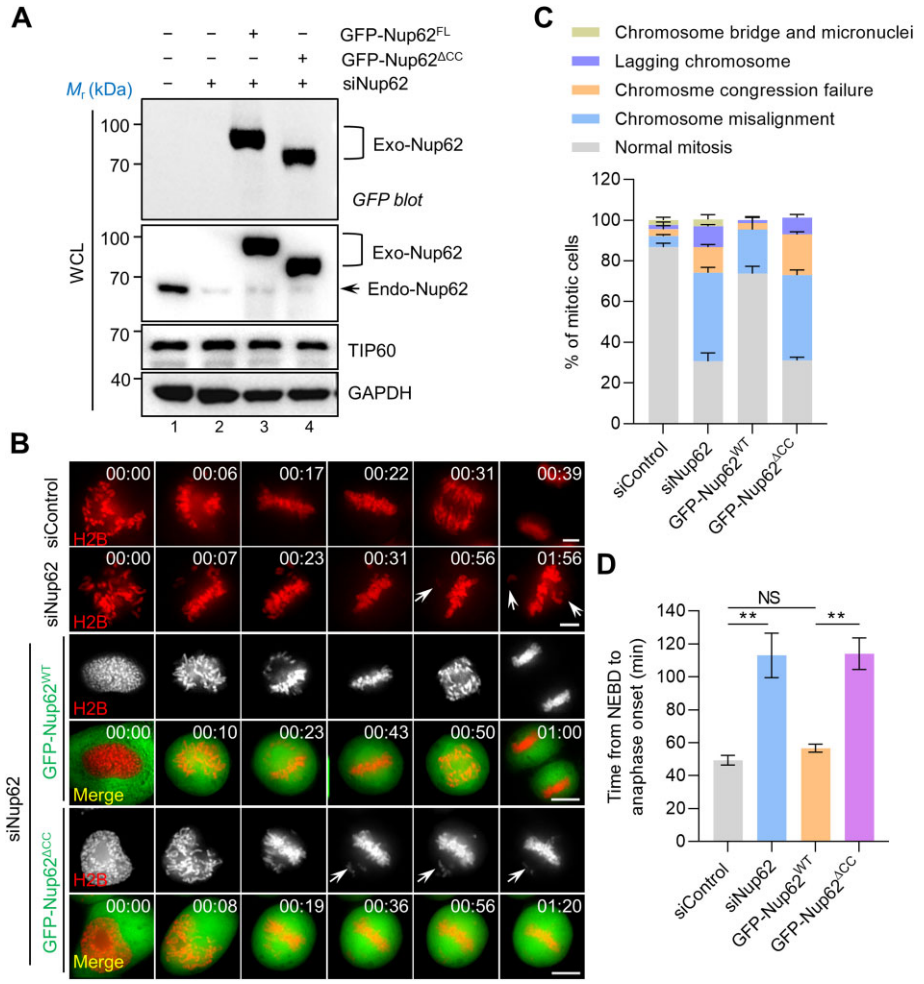

Figure 4 Nup62 is essential for accurate chromosome alignment and faithful segregation. (**A**) HeLa cells were co-transfected with GFP-Nup62^{FL} or GFP-Nup62$^{\Delta CC}$ (siRNA-resistant) plasmids for 24 h with control siRNA or siNup62 for 48 h and analyzed by western blotting. Anti-Nup62 and anti-TIP60 antibodies were probed to show Nup62 (endogenous and exogenous) and TIP60 levels, respectively. GAPDH served as a loading control. (**B**) Nup62-depleted cells were transfected with siRNA-resistant GFP-Nup62^{WT} or GFP-Nup62$^{\Delta CC}$ mutant. mCherry-H2B was co-transfected to indicate chromosome. Representative real-time images of each group are shown. Scale bar, 10 μm. (**C**) Quantification of mitotic phenotype of cells in **B**. At least 60 cells from three separate experiments per group were analyzed. (**D**) Quantification of time intervals from NEBD to anaphase onset in cells of **B**. At least 75 cells from three separate experiments per group were analyzed. Statistical significance was examined by two-sided *t*-test; NS, not significant; $^{**}P < 0.01$.

endogenous Nup62 (Supplementary Figure S4A and B) based on published work (Rodriguez-Berriguete et al., 2018). Importantly, suppression of Nup62 resulted in loss of nuclear rims in significant population of asynchronous cells depleted of Nup62 by siRNA (Supplementary Figure S4C and D).

To rule out the interference of endogenous Nup62 while unraveling the functional importance of Nup62 during mitosis, we suppressed endogenous Nup62 with siRNA and introduced expression constructs resistant to siRNA treatment. As shown in Figure 4A, the exogenous GFP-Nup62 proteins were expressed at a similar level (lanes 3 and 4), which was resistant to siRNA treatment. As shown in Figure 4B, suppression of Nup62 by siRNA treatment exhibited a typical chromosome segregation defect, as a few chromosomes were scattering around the spindle poles with chronic mitotic arrest for >2 h (top panel). As predicted, expression of GFP-Nup62 rescued the phenotype observed in siRNA treatment, as cells progressed into anaphase onset in 50 min (middle panel). However, expression of GFP-Nup62$^{\Delta CC}$ failed to restore accurate chromosome segregation induced by siRNA (bottom panel). Statistical analyses showed that cells expressing GFP-Nup62$^{\Delta CC}$ exhibited a high proportion of chromosome misalignment and abnormal anaphase (Figure 4C). In addition, these GFP-Nup62$^{\Delta CC}$-expressing cells displayed a prolonged interval from NEBD to anaphase onset (Figure 4D), consistent with the phenotypes reported in the literature (Martino et al., 2017). Thus, we conclude that Nup62 interaction with TIP60 is important in mitosis, and its perturbation results in severe mitotic defects.

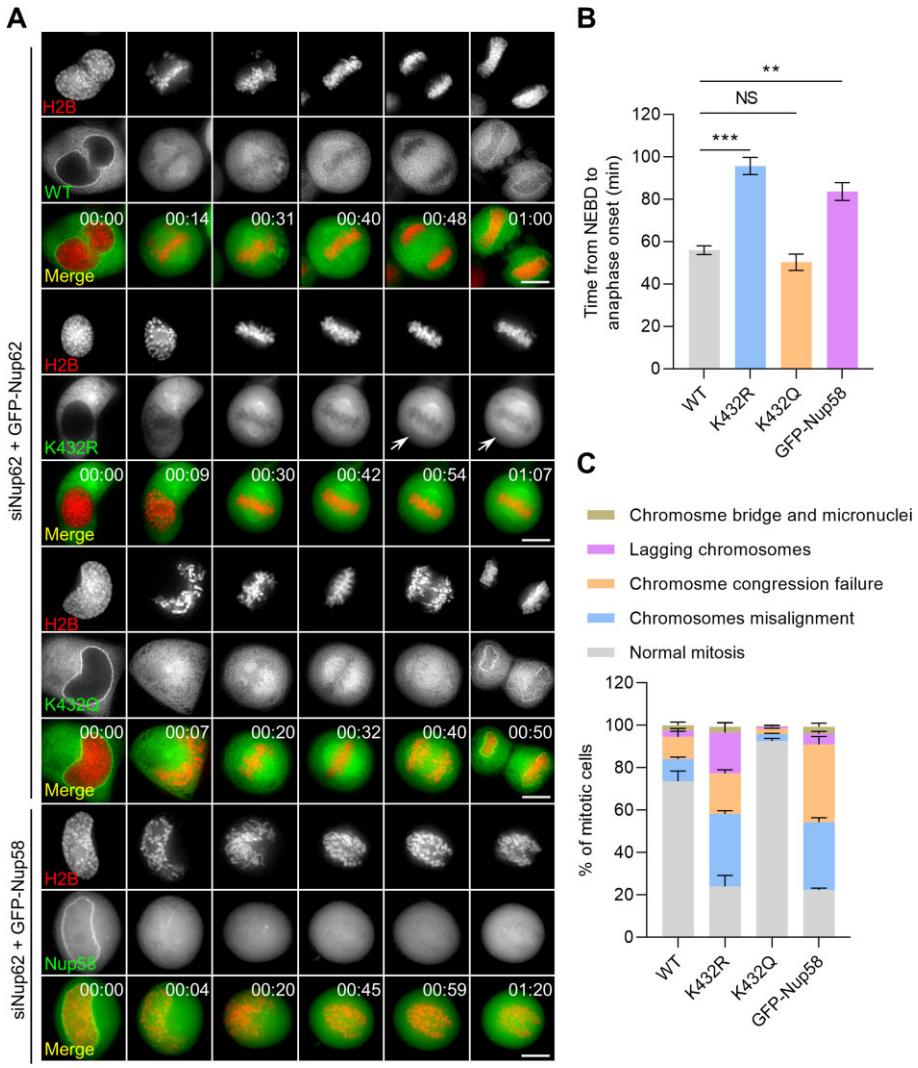

Figure 5 Nup62 acetylation promotes normal mitotic progression. (**A**) Real-time analyses of chromosome movements and mitosis progression in Nup62-depleted cells transfected with GFP-Nup62^{WT}, GFP-Nup62^{K432R}, GFP-Nup62^{K432Q}, and GFP-Nup58, respectively. Scale bar, 10 μm. (**B**) Quantitative analysis of time intervals from NEBD to anaphase onset in HeLa cells. For each group, 75 cells were analyzed. Data represent mean ± SEM from three independent experiments. Statistical significance was tested by two-sided *t*-test; $^{**}P < 0.01$, $^{***}P < 0.001$; NS, not significant. (**C**) Quantification of chromosome dynamics and alignment error phenotypes in **A**. For each group, at least 75 cells were scored.

Nup62 acetylation promotes robust kinetochore–microtubule attachment

To probe whether the acetylation of Lys432 exhibits any physiological function in mitosis, we carried out real-time analyses to examine chromosome segregation dynamics using mCherry-H2B-expressing HeLa cells. Endogenous Nup62 was knocked down, and exogenous siRNA-resistant and non-acetylatable Nup62^{K432R} or acetylation-mimicking Nup62^{K432Q} was expressed, respectively. Western blotting analyses confirmed that the levels of various exogenously expressed GFP-Nup62 proteins (WT, K432R, and K432Q) were comparable in the presence of Nup62 siRNA treatment (Supplementary Figure S5A). As shown in Figure 5A, exogenously expressed GFP-Nup62^{WT} and GFP-Nup62^{K432Q} successfully rescued the phenotypes seen as mitotic arrest and abnormal anaphase resulting from the knockdown of endogenous Nup62. However, non-acetylatable GFP-Nup62^{K432R} failed to rescue the phenotype of cells deficient in endogenous Nup62 (Figure 5A; middle panel). In these GFP-Nup62^{K432R}-expressing cells, apparent spindle orientation defects were seen as the two spindle poles did not exist at the same focal plane (Figure 5A; arrows). To further evaluate whether the observed mitotic perturbation were really due to Nup62 knockdown but not the downregulation or aberrant localization of other Nups in the Nup62 complex (Hartono et al., 2019), we examined the localization dynamics of Nup58 in Nup62-depleted cells in mitosis. Interestingly, GFP-Nup58-expressing cells depleted of Nup62 showed normal localization to NPC in prophase and to centrosome during proceeding phases (Figure 5A; bottom panel). However, the mitotic defects still persisted, similar to that in siNup62-

transfected cells (Figure 4B). More importantly, GFP-Nup58 failed to rescue mitotic aberrant phenotypes like GFP-Nup62^{WT}- or GFP-Nup62^{K432Q}-expressing cells, suggesting that they function in parallel but interactive pathways during mitosis. Quantitative analyses of the intervals from NEBD to anaphase, as shown in Figure 5B, indicated that there was no apparent difference among cells expressing Nup62^{WT} and Nup62^{K432Q}. However, cells expressing Nup62^{K432R} or GFP-Nup58 exhibited chronic delay in mitosis (Figure 5B). In addition, non-acetylatable GFP-Nup62^{K432R} resulted in an increased error rate in chromosome alignment, which was also observed in GFP-Nup58 and siNup62 co-transfected cells (Figure 5C). Consistent with the literature, inhibition of TIP60 by chemical inhibitors such as NU9056 and MG149 also perturbed chromosome segregation (Supplementary Figure S5B and C). Moreover, to seek whether acetylation-mimicking Nup62 can rescue TIP60 inhibition-elicited mitotic defects, a real-time imaging of HeLa cells expressing GFP-tagged Nup62^{K432Q} was performed. Interestingly, acetylation-mimicking Nup62 was able to partially rescue the proportion of cells showing mitotic aberrant phenotypes caused by NU9056 (Supplementary Figure S5D and E), which restored chromosome dynamics and spindle orientation (Supplementary Figure S5D; lower panel) and completed mitosis in $<$1 h (Supplementary Figure S5F). These results suggest that the acetylation of Nup62 by TIP60 regulates accurate mitosis.

Nup62 acetylation functions in spindle orientation

In early mitosis, TIP60 dynamically acetylates Aurora B, Ran, and Hec1 to ensure accurate chromosome segregation and microtubule–kinetochore attachment for accurate metaphase alignment (Mo et al., 2016; Bao et al., 2018; Zhao et al., 2019). In GFP-Nup62^{K432R}-expressing cells, apparent spindle orientation defects were seen as the two spindle poles did not exist at the same focal plane (Figure 5A; middle panel, arrows). To quantify the perturbation of spindle orientation by Nup62^{K432R} expression, Nup62-deficient HeLa cells were transfected with GFP-tagged WT Nup62 and various mutants. These cells were then fixed by cold methanol and co-stained with 4,6-diamidino-2-phenylindole (DAPI). The z-axis images were acquired to generate three-dimensional (3D) image stacks (Figure 6A). The spindle orientation angle α is calculated as previously reported (Yu et al., 2019; Song et al., 2021). Our statistical analyses showed that suppression of Nup62 resulted in spindle mis-orientation. Most Nup62-deficient cells exhibited spindle rotation of $>$10° (Figure 6B and C). Our observation was consistent with a previous study that related Nup62 depletion with spindle mis-orientation (Hashizume et al., 2013).

To quantify the perturbation of spindle orientation by non-acetylatable Nup62^{K432R} expression, Nup62-deficient HeLa cells were transfected with GFP-tagged WT Nup62 and various mutants. These cells were then fixed and co-stained with pericentrin and DAPI (Figure 6D). The z-axis images were acquired to generate 3D image stacks and our statistical analyses showed that most cells expressing GFP-Nup62^{K432R} exhibited spindle rotation of $>$20°, which was distinctly different from those expressing GFP-Nup62^{WT} and GFP-Nup62^{K432Q} (Figure 6E). Thus, we conclude that dynamic acetylation of Nup62 by TIP60 is important for accurate spindle orientation.

Nup62 acetylation is essential for the cortical localization of the LGN–NuMA complex

Accurate spindle orientation determines cell polarity and cell fate in tissue plasticity and homeostasis (Jorgensen and Tyers, 2004; Morin and Bellaïche, 2011; Kiyomitsu and Cheeseman, 2013). LGN–NuMA is an evolutionarily conserved heterotrimeric (Gα protein Gαi, LGN, and NuMA) complex essential for spindle positioning in both vertebrate and invertebrate species (Schaefer et al., 2000; Yu et al., 2000; Lechler and Fuchs, 2005; Morin et al., 2007; Peyre et al., 2011). In HeLa cells, LGN–NuMA symmetrically distributes at the cell cortex for recruitment of the dynein–dynactin complex, which coordinates the astral microtubule to plasma membrane cortex for generating pulling forces to rotate the spindle for optimal capture of kinetochore (Du et al., 2002; Kisurina-Evgenieva et al., 2004; Kotak and Gönczy, 2013; Sun et al., 2021). To determine how the TIP60-elicited acetylated Nup62 disturbs spindle orientation, we first examined the distribution of LGN and NuMA in cells depleted of endogenous Nup62 and expressing siRNA-resistant WT or mutated Nup62 tagged with GFP. Importantly, as shown in Figure 7A and C, the localization of both LGN and NuMA was perturbed at the cell cortex upon Nup62 depletion (compare upper two rows). However, the cortical localization of LGN–NuMA became readily apparent in the Nup62-deficient cells expressing either GFP-Nup62^{WT} or acetylation-mimicking GFP-Nup62^{K432Q} mutant (3rd and 4th rows). Meanwhile, as shown in Figure 7B and D, only less than half of metaphase HeLa cells deficient in endogenous Nup62 without or with GFP-Nup62^{K432R} exhibited obvious enrichment of LGN and NuMA at the cell cortex, respectively. Thus, we conclude that Nup62 acetylation promotes the cortical targeting and the maintenance of LGN–NuMA localization for proper spindle orientation during mitosis.

To prevent spindle mis-orientation, multiple levels of astral microtubule regulation occur, i.e. nucleation of astral microtubules at the centrosomes and plus-end linkage with the cell cortex (di Pietro et al., 2016). Importantly, plus-end linkage with the cortex is mediated by the interaction of cortical proteins including the LGN–NuMA complex with astral microtubules. As acetylation-deficient Nup62 perturbs cortical localization of LGN–NuMA (Figure 7A–D), it should also disrupt astral microtubule linkage with the cell cortex. To examine whether Nup62 knockdown and TIP60-mediated Nup62 acetylation affected astral microtubule length and association with the cell cortex, HeLa cells expressing GFP-Nup62 constructs were stained for α-tubulin and the centrosomal marker protein, pericentrin. As exhibited in Supplementary Figure S6A, astral microtubules reached the cell cortex in the control, contrary to the cells depleted of Nup62, indicating destabilized astral microtubules (top two rows, magnified insets). Astral microtubules in cells depleted of endogenous Nup62 and expressing siRNA-resistant GFP-Nup62 were also observed

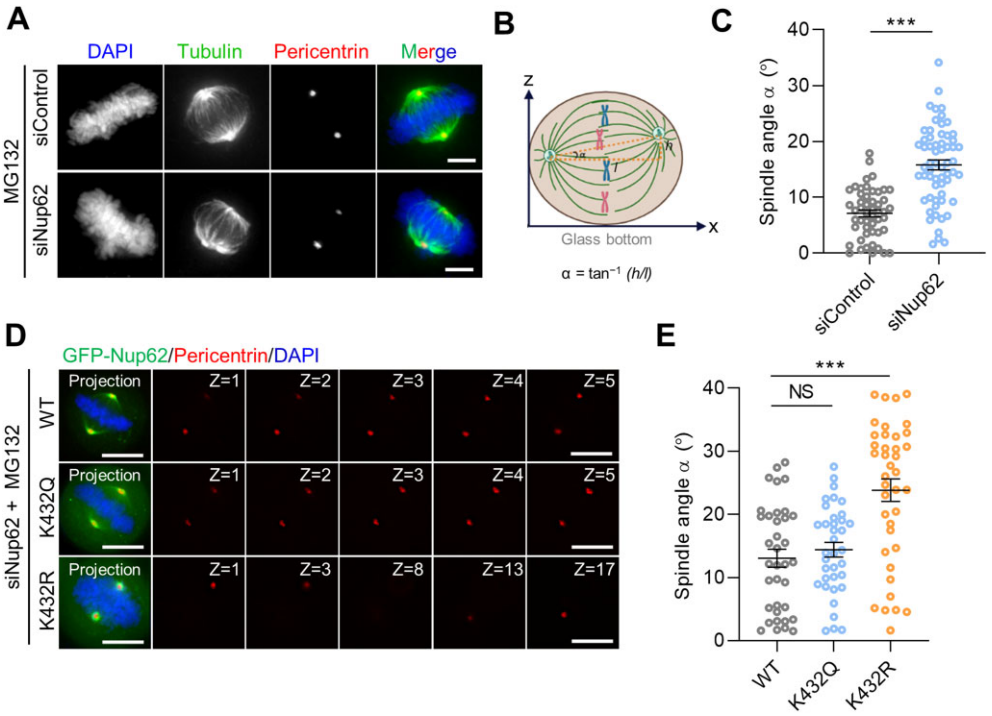

Figure 6 Nup62 acetylation functions in spindle orientation. (**A**) Immunofluorescence images of HeLa cells transfected with siNup62 and synchronized in metaphase for 30 min using MG132. Cells were fixed in cold methanol and stained with anti-pericentrin and anti-tubulin antibodies to indicate centrosome and spindle microtubules, respectively. Chromatin was stained with DAPI. Z-stack projection was performed for images (projection). Scale bar, 5 μm. (**B**) Schematic diagram of spindle angle α measurements. Spindle orientation is represented by the angle α, which is calculated as $\tan^{-1}$ (*h*/*l*). *h* was measured as the distance between the two spindle poles of the cell in the vertical z axis, while *l* was measured as the distance between the two spindle poles in the horizontal plane in the 3D projection. (**C**) Statistical analysis of spindle angle profiles of HeLa cells in **A**. Data represent mean ± SEM from three independent experiments. Statistical significance was tested by two-sided *t*-test; ***$P < 0.001$. (**D**) Immunofluorescence images of Nup62-depleted HeLa cells expressing GFP-Nup62^{WT}, GFP-Nup62^{K432Q}, and GFP-Nup62^{K432R}, respectively. These cells were synchronized in metaphase for 30 min using MG132 before fixation in PTEM buffer. (**E**) Statistical analysis of spindle angle profiles of GFP-Nup62^{WT} and mutants in **D**. For each group, $n = 35$. Data represent mean ± SEM from three independent experiments. The significant difference was evaluated by two-tailed student's *t*-test; ***$P < 0.001$; NS, not significant.

reaching the cell cortex (lower three rows, both insets), which exhibited correct spindle orientation as demonstrated by tubulin and pericentrin staining, respectively. Intriguingly, acetylation-mimicking Nup62^{K432Q}-expressing cells in the absence of endogenous Nup62 efficiently stabilized astral microtubules, like Nup62^{WT}, in majority of metaphase HeLa cells (~70%); however, Nup62^{K432R}-expressing cells failed to restore the linkage of astral microtubules with the cellular cortex (Supplementary Figure S6B). Thus, we conclude that TIP60-mediated Nup62 acetylation is important for stabilizing astral microtubule length and its interaction with the cell cortex.

Discussion

NPC orchestrates nucleocytoplasmic shuttling in interphase cells (Fontana et al., 2022; Huang et al., 2022). In this study, we have identified Nup62 as a novel substrate of TIP60 in mitosis. Nup62 physically interacts with TIP60 both *in vivo* and *in vitro* via its C-terminal region bearing a coiled-coil domain. The TIP60-elicited acetylation of Nup62 at Lys432 plays an important role in the maintenance of centrosome homeostasis, spindle orientation, and orchestrating accurate chromosome alignment and segregation during mitosis.

Nup62 was previously reported for participating in spindle assembly checkpoint, as RNAi-mediated depletion of Nup62 compromised the checkpoint and induced aneuploidy in human neural stem cells (Hashizume et al., 2013). In addition, Nup62 was implicated in centrosome homeostasis, as depletion of Nup62 resulted in perturbation of centrosome maturation, defective MT aster formation, and spindle mis-orientation (Hashizume et al., 2013). Our functional analyses of TIP60-elicited acetylation of Nup62 provide a clue for the contribution of post-translational modifications as a regulatory mechanism of Nup62 in mitosis. It would be of great interest to test whether multiple functions of Nup62 are orchestrated by distinct Nup62 sub-complexes using proximity ligation approach with cell synchronization protocol (Liu et al., 2020).

The spindle is a specialized scaffold architect that orchestrates accurate spindle positioning with the cell cortex, accurate chromosome–microtubule attachment, and spindle assembly checkpoint. Our recent studies of the CDK1–TIP60–EB1

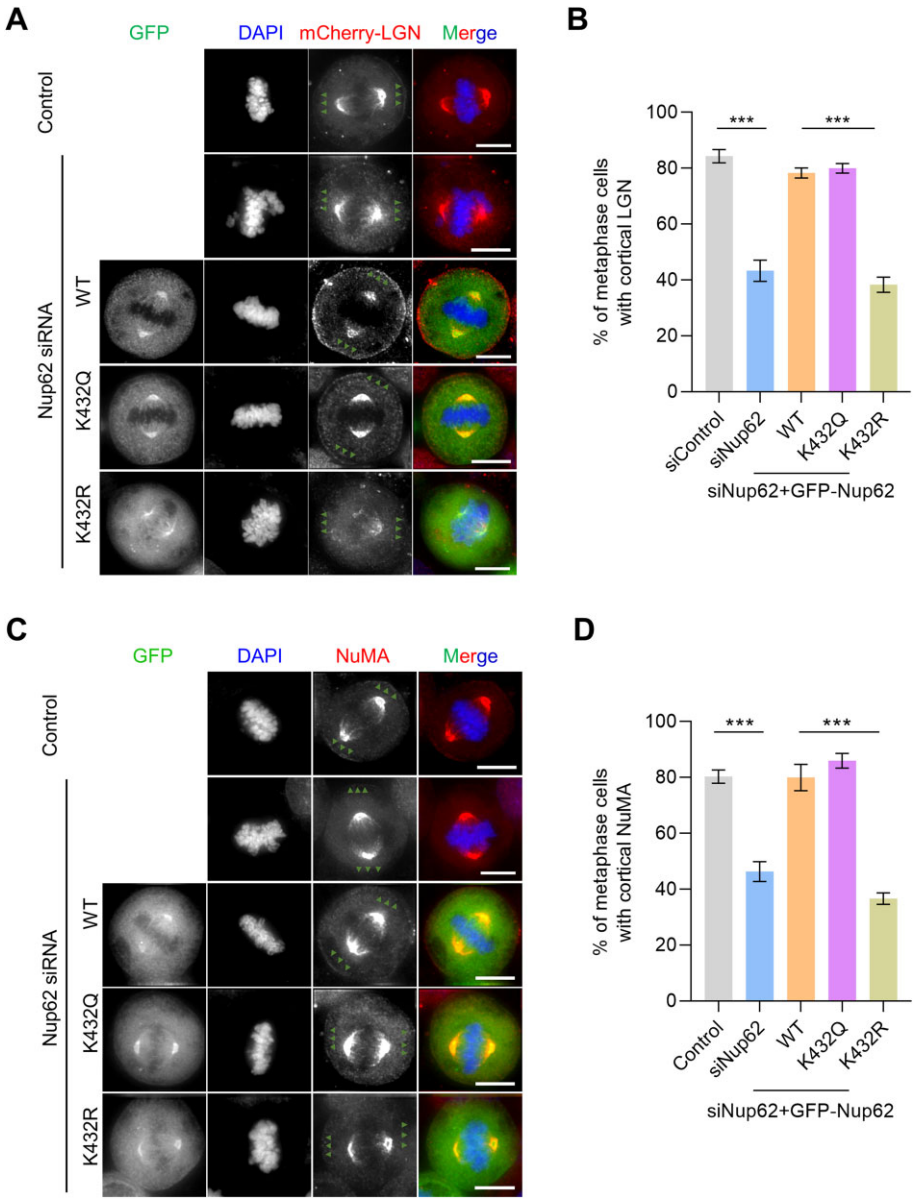

Figure 7 Acetylation of Nup62 by TIP60 is essential for cortical localization of LGN–NuMA. (**A**) Immunofluorescence analyses of mitotic HeLa cells expressing GFP-tagged WT Nup62 or various mutants together with mCherry-LGN and Nup62 siRNA. Cortical localization of LGN is indicated with triangles (green), which is perturbed upon Nup62 depletion. Scale bar, 10 μm. (**B**) Percentage of metaphase cells with obvious enrichment of LGN at the cell cortex in **A**. Data represent mean ± SEM from three independent experiments, $n = 60$ cells for each group. The significant difference was evaluated by two-tailed student's *t*-test; ***$P < 0.001$. (**C**) Immunofluorescence analyses of Nup62-depleted mitotic HeLa cells expressing GFP-Nup62^{WT} or mutants (GFP-Nup62^{K432Q} or GFP-Nup62^{K432R}) using anti-NuMA antibody (red). NuMA localization at the cortex is indicated with triangles (green). Scale bar, 10 μm. (**D**) Percentages of metaphase cells containing cortical NuMA signal as shown in **C**. Data represent mean ± SEM from three independent experiments, $n = 60$ cells for each group. The significant difference was evaluated by two-tailed student's *t*-test; ***$P < 0.001$.

signaling axis delineated a regulatory mechanism by which dynamic crotonylation of EB1 was ensured for accurate spindle orientation (Mo et al., 2016; Song et al., 2021). The fact that TIP60-mediated acetylation of Nup62 regulates spindle plasticity during mitotic chromosome segregation demonstrates that TIP60 exhibits a new acetyltransferase signaling cascade for tuning the spindle positioning for error-free anaphase in mitosis. In the follow-up work, it will be very important to characterize how acetylation of Nup62 is spatiotemporally regulated for the spindle plasticity during mitosis.

Correct spindle positioning during mitosis depends on proper astral microtubule dynamics. It has been shown that the NuMA–LGN complex organizes lateral cortex association with the astral microtubules. Our recent studies established a

previously uncharacterized link between astral microtubules and the NuMA–LGN complex (Song et al., 2021). Since Nup62 and TIP60 are conserved from yeast to human cells, our studies uncovered a highly conserved regulatory mechanism underlying NPC protein family contact with TIP60. Given the critical importance of post-translational crosstalk in mitosis and significance of Lys432 modification in spindle orientation, it would be of great interest to measure the gradient of Ac-CoA vs. Cr-CoA around spindle during mitosis using FRET-based sensors (Chu et al., 2011; Yu et al., 2020).

Our recent molecular delineation of EB1 function in spindle positioning revealed a new EB1–NuMA interaction and an EB1-binding region in NuMA essential for accurate spindle positioning (Song et al., 2021). The newly characterized crotonyl transferase activity of TIP60 is spatiotemporally separated from its activity at the kinetochore during earlier events (Mo et al., 2016), where TIP60–Aurora B interaction at the kinetochores guides accurate chromosome segregation. It is worth noting that Nup62 exhibits spindle pole localization in mitotic cells. Further examination using correlative light electron microscopic analyses would clarify whether Nup62 acetylation results in any abnormalities in spindle pole plasticity.

In sum, our current studies define a new signaling axis that Nup62 integrates spatiotemporal regulation of protein acetylation elicited by TIP60 in mitotic spindle pole to orchestrate accurate chromosome segregation during metaphase–anaphase transition, a process essential for faithful epithelial cell renewal and tissue plasticity. Our study provides great insights into functional relevance of TIP60 interaction with NPCs to ensure faithful chromosome segregation in mitosis.

Materials and methods

Plasmids, siRNA, shRNA, and transfection

The WT human TIP60 and Nup62 constructs were generated by recombination method whereby both genes (TIP60/Nup62) were inserted in to the p3×FLAG-myc-CMV-24 (Sigma-Aldrich) and pEGFP-C1 (Clontech) vectors, respectively, after amplified by polymerase chain reaction (PCR) and recombined according to Vazyme C214 user manual. The bacterial-expressed plasmids of Nup62 and TIP60 used in this work were cloned into pMal-C2 vector (New England Biolabs) and pGEX-6P-1 (GE Healthcare) vector, respectively. All site and deletion mutants of Nup62 were generated by PCR-based mutagenesis approach using the Vazyme mutagenesis Kit (C214-01, Vazyme Inc.). All the plasmids constructed were immediately sequenced for verification. The sense strand sequence of the siRNA was as follow: 5′-GCAAGAUCCUCAAUGCGCA-3′ (Rodriguez-Berriguete et al., 2018). Cells expressing TIP60 shRNA were established by using lentivirus-based system as previously described (Mo et al., 2016). For this purpose, TIP60-targeted sequence (5′-TCGAATTGTTTGGGCACTGAT-3′) was inserted into a lentivirus-based shuttle vector, i.e. PLKO.1 vector (Addgene), which was co-transfected for 72 h with pMD2.G and psPAX2 (two packing plasmids from Addgene) into HEK293T cells to generate lenti-virus. Then, the supernatant containing packaged virus was collected and used to transduce HeLa cells when TIP60 depletion was required. All the plasmids were usually transfected using Lipofectamine 2000 or Lipofectamine 3000 (Invitrogen), and for siRNA, RNAiMax (Invitrogen) was used according to the manufacturer's instructions.

Cell culture, synchronization, and drug treatments

HEK293T and HeLa cells were routinely maintained in advanced DMEM (Invitrogen) with 10% (*v/v*) fetal bovine serum (FBS) (HyClone) and 100 units/ml of penicillin plus 100 μg/ml streptomycin (Gibco). To enrich mitotic cells, HeLa cells were treated with 2.5 mM thymidine (Invitrogen) for 16 h followed by release into a fresh DMEM medium for indicated hours. For NU9056 (20 μM, Tocris Bioscience) treatment, the drug was added into the culture medium after 8-h release from G1/S arrest and maintained for 1 h before and during real-time imaging. HeLa cells were synchronized in metaphase with MG132 (20 μM, Sigma) treatment for spindle angle measurement. For IP of FLAG and GFP-tagged proteins, HEK293T or HeLa cells were treated with nocodazole (100 ng/ml) for 16 h and then harvested for experiments.

Antibodies

Rabbit anti-Nup62 (PA5-21882, Invitrogen), mouse anti-Nup62 monoclonal (sc-48389, Santa Cruz), rabbit anti-TIP60 (10827-1-AP, Proteintech), mouse anti-tubulin (3873, Cell Signaling Technology), rabbit anti-GFP (50430-2-AP, Proteintech), mouse anti-MBP (2396, Cell Signaling Technology), mouse anti-GAPDH (D4C6R, Cell Signaling Technology), mouse anti-FLAG (F3165, Sigma), anti-Cyclin B1 (12231, Cell Signaling Technology), anti-Aurora B (611082, BD), anti-Pericentrin (4448, Abcam), and human ACA (HCT-0100, Immunovision) were obtained commercially. For all western blotting, signals were detected using horseradish peroxidase-conjugated anti-mouse or anti-rabbit antibodies (Pierce).

In vitro acetylation assay

The *in vitro* acetylation assay between indicated proteins was carried out as described previously (Xia et al., 2012). Briefly, either FLAG-TIP60-enriched M2 beads or eluted FLAG-TIP60 was incubated with soluble MBP-Nup62 in 60 μl of HAT buffer (20 mM Tris-HCl, pH 8.0, 1 mM DTT, 10% glycerol, 1 mM EDTA, 10 μM TSA, 100 mM NaCl, and 10 mM NAM) containing 100 μM acetyl-CoA at 37°C for 2 h under a constant and steady agitation. The samples were boiled for 5 min at 95°C after the reaction was stopped by adding 5× sample buffer. Samples were analyzed by western blotting analyses with indicated antibodies.

Immunofluorescence microscopy, image processing, and quantification

For immunofluorescence experiments, HeLa cells were grown on coverslips and transfected with the indicated plasmids before being fixed and permeabilized simultaneously with PTEM buffer (50 mM Pipes, pH 6.8, 0.2% Triton X-100, 1 mM $MgCl_2$, and 10 mM EGTA) supplemented with 4% paraformaldehyde at

room temperature followed by blocking with 1% bovine serum albumin (Sigma) for 1 h at room temperature. Primary and secondary antibodies were sequentially incubated overnight at 4°C and for 1 h at room temperature, respectively, followed by DNA staining with DAPI (Sigma). Finally, coverslips were sealed with nail polish after mounted onto glass slide with antifade mounting medium. Images of the samples were acquired with DeltaVision microscope (Applied Precision) using a 60× objective lens, NA = 1.42, with optical sections of 0.20 μm apart in the z-axis. Spindle orientation, which is represented by the angle α, was calculated as $\tan^{-1}$ (h/l). Usually, l was measured as the inter spindle pole distance in the horizontal plane in the 3D projection, while h was measured as the inter spindle pole distance of the cell in the vertical z-axis. For spindle angle measurement, optical sections were acquired with 0.1 μm apart in the z-axis. The original deconvoluted images were processed by deconvolution and z-stack projection with the help of softWoRx (Applied Precision). Images were mounted into figures with Adobe Photoshop.

Live cell imaging

HeLa cells were cultured and maintained in glass-bottomed culture dishes (MatTek) at 37°C in CO_2-independent medium (Gibco) supplemented with 2 mM glutamine and 10% FBS (v/v) for live cell imaging. Small-molecule inhibitor were added 1 h before and were kept in the medium during image acquisition by DeltaVision microscope (Applied Precision). Images for mitotic cells with optical section of 0.2 μm apart were acquired at 3- or 5-min intervals using live cell system in a DeltaVision deconvolution microscope system (Applied Precision). For imaging, a 60× 1.42 NA objective lens was used. Final images were obtained by projecting all single optical sections into one as described previously (Mo et al., 2016). Images were mounted into figures and prepared for publication using Adobe Photoshop.

Recombinant protein preparation and purification

Plasmids of GST, MBP, GST-TIP60, MBP-Nup62 FL, and MBP-Nup62 mutants were transformed into *Escherichia coli* strain BL21 (DE3), and protein expression was induced at a standard cell density (optical density ∼0.6) at 16°C for 16 h with 0.2 mM IPTG. Bacteria expressing MBP-Nup62 were lysed by sonication in MBP lysis buffer (20 mM Tris-HCl, pH 7.4, 1 mM EDTA, 200 mM NaCl, and 0.1% Triton X-100) supplemented with protease inhibitor cocktail (Sigma) and incubated with amylose resin (New England Biolabs) for 2 h at 4°C. The resin was washed three times with the same buffer adjunct with 0.2% Triton X-100 and eluted with MBP buffer supplemented with 10 mM maltose. Bacterially expressed recombinant proteins of GST-TIP60 and GST were lysed in phosphate-buffered saline (PBS) buffer supplemented with 0.1% Triton X-100 and incubated with glutathione-Sepharose 4B (GE Healthcare Life Science) for 2 h at 4°C. GST-TIP60 and GST protein were eluted with 20 mM glutathione when necessary or kept on the beads for pull-down assay. All purification procedures were performed at 4°C, and a protease inhibitor cocktail (Sigma) was added to prevent protein degradation.

IP and pull-down assay

For FLAG IP, HEK293T cells expressing FLAG-TIP60, GFP-Nup62 (and all mutants), and GFP were lysed in IP buffer (50 mM HEPES, 150 mM NaCl, 2 mM EDTA, pH 7.4) supplemented with 0.1% Triton X-100 plus protease inhibitor cocktail and incubated with anti-FLAG M2 resin for 4 h followed by washing three times with IP buffer adjunct with 0.2% Triton X-100. The binding fractions were analyzed by western blotting with anti-GFP and anti-FLAG antibodies.

The pull-down assay with purified GST-TIP60 and MBP-Nup62 was performed as previously described (Xu et al., 2021). Briefly, GST-TIP60 or GST alone purified on glutathione beads was used as an affinity matrix for absorbing MBP or MBP-Nup62 in the pull-down buffer containing PBS, pH 7.4, EDTA (1 mM), 0.1% Triton X-100, protease cocktail inhibitor, and PMSF (1 mM) for 3 h at 4°C. The beads were washed three times with PBS supplemented with 0.1% Triton X-100 and one time with PBS alone, and then boiled for 5 min in sodium dodecylsulfate–polyacrylamide gel electrophoresis (SDS–PAGE) sample buffer. Proteins were resolved by SDS–PAGE for CBB staining and western blotting analyses.

Statistics

All statistics were described in the figure legends. The Two-tailed unpaired Student's *t*-test was applied for experimental comparisons, using GraphPad Prism 7. No statistical method was used to predetermine sample size. All data were expected to have normal distribution.

Supplementary material

Supplementary material is available at *Journal of Molecular Cell Biology* online.

Acknowledgements

We are grateful to members in our group for assistance and discussion.

Funding

This work was supported by grants from the National Key Research and Development Program of China (2017YFA0503600 and 2016YFA0100500), the National Natural Science Foundation of China (31621002, 32090040, 91854203, 21922706, 91853115, 92153302, 22177106, 92053104, 31970655, and 32100612), the Ministry of Education (IRT_17R102), Anhui Provincial Natural Science Foundation (2108085J15), the Strategic Priority Research Program of the Chinese Academy of Sciences (XDB19040000), and the Fundamental Research Funds for the Central Universities (WK2070000066 and WK2070000194).

Conflict of interest: none declared.

Author contributions: conceptualization: X. Yao and Xing Liu. Investigation: H.A., X. Yuan, M.Z., J.C., X.S., Xu Liu, D.W., and X.G.

Data analysis: H.A., S.M., F.A., and Xing Liu. Funding acquisition: Xing Liu. Supervision: X. Yao and Xing Liu.

References

Alber, F., Dokudovskaya, S., Veenhoff, L.M., et al. (2007). The molecular architecture of the nuclear pore complex. Nature *450*, 695–701.

Bailer, S.M., Balduf, C., and Hurt, E. (2001). The Nsp1p carboxy-terminal domain is organized into functionally distinct coiled-coil regions required for assembly of nucleoporin subcomplexes and nucleocytoplasmic transport. Mol. Cell. Biol. *21*, 7944–7955.

Bao, X., Liu, H., Liu, X., et al. (2018). Mitosis-specific acetylation tunes Ran effector binding for chromosome segregation. J. Mol. Cell Biol. *10*, 18–32.

Chu, Y., Yao, P.Y., Wang, W., et al. (2011). Aurora B kinase activation requires survivin priming phosphorylation by PLK1. J. Mol. Cell Biol. *3*, 260–267.

Clarke, P.R., and Zhang, C. (2008). Spatial and temporal coordination of mitosis by Ran GTPase. Nat. Rev. Mol. Cell Biol. *9*, 464–477.

Devos, D., Dokudovskaya, S., Williams, R., et al. (2006). Simple fold composition and modular architecture of the nuclear pore complex. Proc. Natl Acad. Sci. USA *103*, 2172–2177.

di Pietro, F., Echard, A., and Morin, X. (2016). Regulation of mitotic spindle orientation: an integrated view. EMBO Rep. *17*, 1106–1130.

Dou, Z., Prifti, D.K., Gui, P., et al. (2019). Recent progress on the localization of the spindle assembly checkpoint machinery to kinetochores. Cells *8*, E278.

Du, Q., Taylor, L., Compton, D.A., et al. (2002). LGN blocks the ability of NuMA to bind and stabilize microtubules. A mechanism for mitotic spindle assembly regulation. Curr. Biol. *12*, 1928–1933.

Echeverría, P.C., Mazaira, G., Erlejman, A., et al. (2009). Nuclear import of the glucocorticoid receptor–hsp90 complex through the nuclear pore complex is mediated by its interaction with Nup62 and importin β. Mol. Cell. Biol. *29*, 4788–4797.

Fontana, P., Dong, Y., Pi, X., et al. (2022). Structure of cytoplasmic ring of nuclear pore complex by integrative cryo-EM and AlphaFold. Science *376*, eabm9326.

Güttinger, S., Laurell, E., and Kutay, U. (2009). Orchestrating nuclear envelope disassembly and reassembly during mitosis. Nat. Rev. Mol. Cell Biol. *10*, 178–191.

Hartono, Hazawa, M., Lim, K.S., et al. (2019). Nucleoporin Nup58 localizes to centrosomes and mid-bodies during mitosis. Cell Div. *14*, 7.

Hashizume, C., Moyori, A., Kobayashi, A., et al. (2013). Nucleoporin Nup62 maintains centrosome homeostasis. Cell Cycle *12*, 3804–3816.

Huang, G., Zhan, X., Zeng, C., et al. (2022). Cryo-EM structure of the inner ring from the Xenopus laevis nuclear pore complex. Cell Res. *32*, 451–460.

Hubert, T., Vandekerckhove, J., and Gettemans, J. (2009). Exo70-mediated recruitment of nucleoporin Nup62 at the leading edge of migrating cells is required for cell migration. Traffic *10*, 1257–1271.

Jorgensen, P., and Tyers, M. (2004). How cells coordinate growth and division. Curr. Biol. *14*, R1014–R1027.

Jovanovic-Talisman, T., Tetenbaum-Novatt, J., McKenney, A.S., et al. (2009). Artificial nanopores that mimic the transport selectivity of the nuclear pore complex. Nature *457*, 1023–1027.

Kisurina-Evgenieva, O., Mack, G., Du, Q., et al. (2004). Multiple mechanisms regulate NuMA dynamics at spindle poles. J. Cell Sci. *117*, 6391–6400.

Kiyomitsu, T., and Cheeseman, I.M. (2013). Cortical dynein and asymmetric membrane elongation coordinately position the spindle in anaphase. Cell *154*, 391–402.

Kotak, S., and Gönczy, P. (2013). Mechanisms of spindle positioning: cortical force generators in the limelight. Curr. Opin. Cell Biol. *25*, 741–748.

Krupina, K., Goginashvili, A., and Cleveland, D.W. (2021). Causes and consequences of micronuclei. Curr. Opin. Cell Biol. *70*, 91–99.

Lechler, T., and Fuchs, E. (2005). Asymmetric cell divisions promote stratification and differentiation of mammalian skin. Nature *437*, 275–280.

Leng, Y., Cao, C., Ren, J., et al. (2007). Nuclear import of the MUC1-C oncoprotein is mediated by nucleoporin Nup62. J. Biol. Chem. *282*, 19321–19330.

Linder, M.I., Köhler, M., Boersema, P., et al. (2017). Mitotic disassembly of nuclear pore complexes involves CDK1- and PLK1-mediated phosphorylation of key interconnecting nucleoporins. Dev. Cell *43*, 141–156.e7.

Liu, X., Liu, X., Wang, H., et al. (2020). Phase separation drives decision making in cell division. J. Biol. Chem. *295*, 13419–13431.

Makiyama, K., Hazawa, M., Kobayashi, A., et al. (2022). NSP9 of SARS-CoV-2 attenuates nuclear transport by hampering nucleoporin 62 dynamics and functions in host cells. Biochem. Biophys. Res. Commun. *586*, 137–142.

Martino, L., Morchoisne-Bolhy, S., Cheerambathur, D.K., et al. (2017). Channel nucleoporins recruit PLK-1 to nuclear pore complexes to direct nuclear envelope breakdown in C. elegans. Dev. Cell *43*, 157–171.e7.

Mo, F., Zhuang, X., Liu, X., et al. (2016). Acetylation of Aurora B by TIP60 ensures accurate chromosomal segregation. Nat. Chem. Biol. *12*, 226–232.

Monette, A., Panté, N., and Mouland, A.J. (2011). HIV-1 remodels the nuclear pore complex. J. Cell Biol. *193*, 619–631.

Morin, X., and Bellaïche, Y. (2011). Mitotic spindle orientation in asymmetric and symmetric cell divisions during animal development. Dev. Cell *21*, 102–119.

Morin, X., Jaouen, F., and Durbec, P. (2007). Control of planar divisions by the G-protein regulator LGN maintains progenitors in the chick neuroepithelium. Nat. Neurosci. *10*, 1440–1448.

Peyre, E., Jaouen, F., Saadaoui, M., et al. (2011). A lateral belt of cortical LGN and NuMA guides mitotic spindle movements and planar division in neuroepithelial cells. J. Cell Biol. *193*, 141–154.

Rodriguez-Berriguete, G., Granata, G., Puliyadi, R., et al. (2018). Nucleoporin 54 contributes to homologous recombination repair and post-replicative DNA integrity. Nucleic Acids Res. *46*, 7731–7746.

Schaefer, M., Shevchenko, A., Shevchenko, A., et al. (2000). A protein complex containing Inscuteable and the Gα-binding protein Pins orients asymmetric cell divisions in Drosophila. Curr. Biol. *10*, 353–362.

Sheffield, L.G., Miskiewicz, H.B., Tannenbaum, L.B., et al. (2006). Nuclear pore complex proteins in Alzheimer disease. J. Neuropathol. Exp. Neurol. *65*, 45–54.

Song, X., Yang, F., Liu, X., et al. (2021). Dynamic crotonylation of EB1 by TIP60 ensures accurate spindle positioning in mitosis. Nat. Chem. Biol. *17*, 1314–1323.

Sun, M., Jia, M., Ren, H., et al. (2021). NuMA regulates mitotic spindle assembly, structural dynamics, and function via phase separation. Nat. Commun. *12*, 7157.

Ungricht, R., and Kutay, U. (2017). Mechanisms and functions of nuclear envelope remodelling. Nat. Rev. Mol. Cell Biol. *18*, 229–245.

Walther, T.C., Alves, A., Pickersgill, H., et al. (2003). The conserved Nup107–160 complex is critical for nuclear pore complex assembly. Cell *113*, 195–206.

Xia, P., Wang, Z., Liu, X., et al. (2012). EB1 acetylation by P300/CBP-associated factor (PCAF) ensures accurate kinetochore–microtubule interactions in mitosis. Proc. Natl Acad. Sci. USA *109*, 16564–16569.

Xu, L., Ali, M., Duan, W., et al. (2021). Feedback control of PLK1 by Apolo1 ensures accurate chromosome segregation. Cell Rep. *36*, 109343.

Yu, F., Morin, X., Cai, Y., et al. (2000). Analysis of partner of inscuteable, a novel player of Drosophila asymmetric divisions, reveals two distinct steps in inscuteable apical localization. Cell *100*, 399–409.

Yu, H., Yang, F., Dong, P., et al. (2019). NDP52 tunes cortical actin interaction with astral microtubules for accurate spindle orientation. Cell Res. *29*, 666–679.

Yu, R., Wu, H., Ismail, H., et al. (2020). Methylation of PLK1 by SET7/9 ensures accurate kinetochore–microtubule dynamics. J. Mol. Cell Biol. *12*, 462–476.

Zhao, G., Cheng, Y., Gui, P., et al. (2019). Dynamic acetylation of the kinetochore-associated protein HEC1 ensures accurate microtubule–kinetochore attachment. J. Biol. Chem. *294*, 576–592.